CrossMark

ORIGINAL ARTICLE

Low-temperature growth of nitrogen-doped carbon nanofibers by acetonitrile catalytic CVD using Ni-based catalysts

Tomohiro Iwasaki[1] · Yuri Makino[1] · Makoto Fukukawa[1] · Hideya Nakamura[1] · Satoru Watano[1]

Abstract To synthesize nitrogen-doped carbon nanofibers (N-CNFs) at high growth rates and low temperatures less than 673 K, nickel species (metallic nickel and nickel oxide) supported on alumina particles were used as the catalysts for an acetonitrile catalytic chemical vapor deposition (CVD) process. The nickel:alumina mass ratio in the catalysts was fixed at 0.05:1. The catalyst precursors were prepared from various nickel salts (nitrate, chloride, sulfate, acetate, and lactate) and then calcined at 1073 K for 1 h in oxidative (air), reductive (hydrogen-containing argon), or inert (pure argon) atmospheres to activate the nickel-based catalysts. The effects of precursors and calcination atmosphere on the catalyst activity at low temperatures were studied. We found that the catalysts derived from nickel nitrate had relatively small crystallite sizes of nickel species and provided N-CNFs at high growth rates of 57 ± 4 g-CNF/g-Ni/h at 673 K in the CVD process using 10 vol% hydrogen-containing argon as the carrier gas of acetonitrile vapor, which were approximately 4 times larger than that of a conventional CVD process. The obtained results reveal that nitrate ions in the catalyst precursor and hydrogen in the carrier gas can contribute effectively to the activation of catalysts in low-temperature CVD. The fiber diameter and nitrogen content of N-CNFs synthesized at high growth rates were several tens of nanometers and 3.5 ± 0.3 at.%, respectively. Our catalysts and CVD process may lead to cost reductions in the production of N-CNFs.

✉ Tomohiro Iwasaki
   iwasaki@chemeng.osakafu-u.ac.jp

[1] Department of Chemical Engineering, Osaka Prefecture University, Sakai, Osaka 599-8531, Japan

Introduction

The use of carbon nanofibers (CNFs) is being expanded to improve the performance of industrial products, such as batteries, supercapacitors, solar cells, sensors, catalysts, and adsorbents, because CNFs have excellent electrical, thermal, mechanical, and physicochemical properties resulting from their unique carbon nanostructure and morphologies (Desmaris et al. 2015; Feng et al. 2014; Jiang 2014; Peng et al. 2016; Song and Shen 2014; Zhang et al. 2014, 2016). Recently, the biocompatibility of CNFs has attracted attention, and the biomedical applications of CNFs [e.g., bone regeneration, biosensors, and antibiotic materials (Ashfaq et al. 2016; Erdem et al. 2015; Gao et al. 2016; Stout 2015; Zhang et al. 2014)] have increased. Furthermore, to enhance properties of CNFs and/or to add new functionality to CNFs, the doping of heteroatoms into CNFs has been employed. In particular, nitrogen-doped carbon nanofibers (N-CNFs) have been actively studied for various purposes, such as electrochemical applications with oxygen reduction catalysts (Buan et al. 2016; Cheng et al. 2015; Kim et al. 2016).

Several methods for synthesizing N-CNFs have been developed so far. Among them, catalytic chemical vapor deposition (CCVD) using a fixed or fluidized bed reactor has been widely employed because of simplicity in the process. In many N-CNF production processes with CCVD, nitrogen doping treatments are performed in an additional process after the formation of CNFs, which can complicate the production process. However, the use of hydrocarbon-containing nitrogen (e.g., acetonitrile) as the carbon source

مدينة الملك عبدالعزيز
KACST للعلوم والتقنية

🍃 Springer

in the CCVD can lead to nitrogen doping of the CNFs as well as CNF growth. Thus, such simple one-step processes may be suitable for the industrial production of N-CNFs, but they must be operated at high temperatures to increase the catalytic activity, which may lead to increased energy costs and reductions in the reactor life. To overcome such drawbacks, high-efficiency production of N-CNFs at low temperatures is required. Lim and co-workers synthesized N-CNFs at low temperatures less than 500 °C using a magnesium oxide-supported nickel–iron catalyst; however, the growth rates were relatively low (Kim et al. 2011; Lim et al. 2009). To the best of our knowledge, there is no study focusing on low-temperature growth of N-CNFs.

Therefore, in this study, we have developed nickel-based catalysts with high activity even at low temperatures less than 400 °C to improve the growth rate of N-CNFs in CCVD. Metallic nickel and/or nickel oxide supported on alumina particles was employed as the catalyst to simplify the catalyst preparation process and to reduce the cost of materials. The effects on the growth rate of counter anions in the catalyst precursors (nickel salts) and calcination atmospheres in the catalyst activation were studied.

Experimental

Chemicals

As the nickel source for the preparation of catalyst precursors, nickel salts with different counter anions, such as nickel nitrate hexahydrate ($Ni(NO_3)_2 \cdot 6H_2O$), nickel chloride hexahydrate ($NiCl_2 \cdot 6H_2O$), nickel sulfate hexahydrate ($NiSO_4 \cdot 6H_2O$), nickel acetate tetrahydrate ($Ni(CH_3COO)_2 \cdot 4H_2O$) (Wako Pure Chemical Industries), and nickel lactate trihydrate ($Ni(C_3H_5O_3)_2 \cdot 3H_2O$) (Mitsuwa Chemicals) were used. Alumina (α-Al_2O_3) powder with an average diameter of 1.8 μm (Wako Pure Chemical Industries) was employed as the catalyst support. Ethanol as the solvent for nickel salts and acetonitrile as the carbon and nitrogen source in CVD were purchased from Kishida Chemical and Wako Pure Chemical Industries, respectively. Pure argon and 10 vol% hydrogen-containing argon (denoted as 10 %H_2/Ar hereafter) were obtained from Air Liquide Kogyo Gas. All of the chemicals used in this study were used without further purification.

Preparation of catalysts

The Ni-based catalyst powders were prepared via a wet impregnation method according to the literature (Liu and Harris 2010) with a slight modification. Briefly, a predetermined amount of a nickel salt was dissolved in 16 mL of either deionized water (for $NiSO_4 \cdot 6H_2O$) or ethanol (for the

others), and then 1 g of the alumina powder was added to the solution. The Ni:Al_2O_3 mass ratio was fixed at 0.05:1 in all of the catalysts. After sonication (40 W) for 5 min, the suspension was dried at 110 °C for 24 h to evaporate the solvent. The dried catalyst precursor powder was activated by calcination at 800 °C for 1 h. The calcination was performed in oxidative (static air in an oven), reductive (a constant flow of 400 standard cubic centimeters per minute (sccm) of 10 %H_2/Ar), and inert (400 sccm of pure Ar) atmospheres. The resulting powder was disintegrated using a mortar and pestle for 20 min and used as the catalyst in the CVD process afterward. Hereafter, the catalysts thus prepared were denoted as X–Y, where X represents the nickel salt used in the preparation of precursors [i.e., X = N (nitrate), C (chloride), S (sulfate), A (acetate), and L (lactate)] and Y represents the calcination atmosphere [i.e., Y = O (oxidative: air), R (reductive: 10 vol % H_2/Ar), and I (inert: Ar)]. For example, N–R indicates a catalyst derived from $Ni(NO_3)_2$ precursor calcined in 10 %H_2/Ar.

Formation of N-doped CNFs

N-doped CNFs were synthesized in a fixed-bed CVD process using acetonitrile as both the carbon and nitrogen source (Iwasaki et al. 2013, 2015). Approximately 0.1 g of a catalyst powder was spread onto an alumina substrate (boat) and then placed in a quartz reaction tube with an inner diameter of 18 mm. The quartz tube was placed horizontally in an electric tube furnace coupled to a PID temperature controller. The furnace temperature was increased to a CVD reaction temperature of 400 °C at a constant rate of 10 °C/min, and then, acetonitrile vapor, which was produced by passing the carrier gas (10 %H_2/Ar) at 400 sccm through acetonitrile at room temperature, was supplied into the quartz tube. The acetonitrile vapor supply was maintained for 15 min (i.e., CVD reaction time). After that, the furnace was allowed to cool to room temperature in the carrier gas flow without acetonitrile. The pressure in the quartz tube was maintained at atmospheric pressure in all of the experiments. Finally, the alumina substrate with the catalyst and product was removed from the quartz tube, and the deposits were weighed and characterized. To study the effect of H_2 in the carrier gas on the growth of N-CNFs in the CVD process, pure Ar was used instead of 10 %H_2/Ar as the carrier gas in the CVD experiments using the N–O, N–R, and N–I catalysts. In addition, the N–O, N–R, and N–I catalysts were subjected to the CVD process using the 10 %H_2/Ar carrier gas without acetonitrile vapor to confirm the change of Ni species (e.g., metallic Ni and NiO) in the catalysts during CVD. Furthermore, to investigate the temperature dependence of the growth rate and properties of N-CNFs, the CVD experiments using the N–R catalyst were performed at temperatures between 300 and 500 °C.
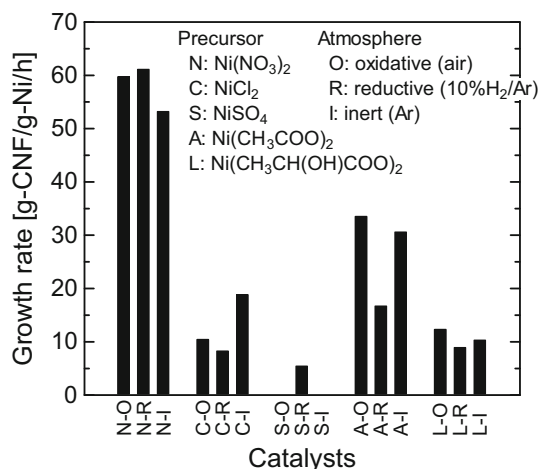
Fig. 1 Effect of catalyst precursors and activation atmospheres on growth rate of N-CNFs at 400 °C

Characterization

The growth rate of N-CNFs was defined as the increased mass of catalyst divided by the mass of nickel (catalytic component) in the catalyst per 1 h (i.e., unit of growth rate: g-CNF/g-Ni/h). The morphology of N-CNFs was imaged by field emission scanning electron microscopy (FE-SEM; JSM-6700F, JEOL) operated at an accelerating voltage of 15 kV. The powder X-ray diffraction (XRD) patterns of catalysts and products were obtained on an X-ray diffractometer (RINT-1500, Rigaku; CuKα radiation, 40 kV, 80 mA). The average crystallite sizes of metallic Ni and NiO in the catalysts were determined using Scherrer's equation for the diffraction peaks from the Ni(111) plane at $2\theta \approx 44°$ and the NiO(220) plane at $2\theta \approx 63°$, respectively. The interlayer spacing d_{002} between graphite sheets in the N-CNFs was also calculated using Bragg's law for the diffraction peak from the C(002) plane at $2\theta \approx 26°$. Furthermore, the carbon and nitrogen contents of N-CNFs were determined based on combustion in oxygen using a CHN elemental analyzer (2400 Series II, PerkinElmer). The nitrogen content was calculated using the formula 100 N/(C + N), where N and C indicate the atomic percent of nitrogen and carbon, respectively. The TG/DTA curves were measured with a thermogravimetric and differential thermal analyzer (DTG-60, Shimadzu; 10 °C/min, air flow at 100 mL/min) to confirm the amorphous carbon in the products.

Results and discussion

Effect of precursor and calcination atmosphere on catalyst activity

Figure 1 shows the growth rate of N-CNFs in CVD at 400 °C for different catalysts. When the catalysts derived
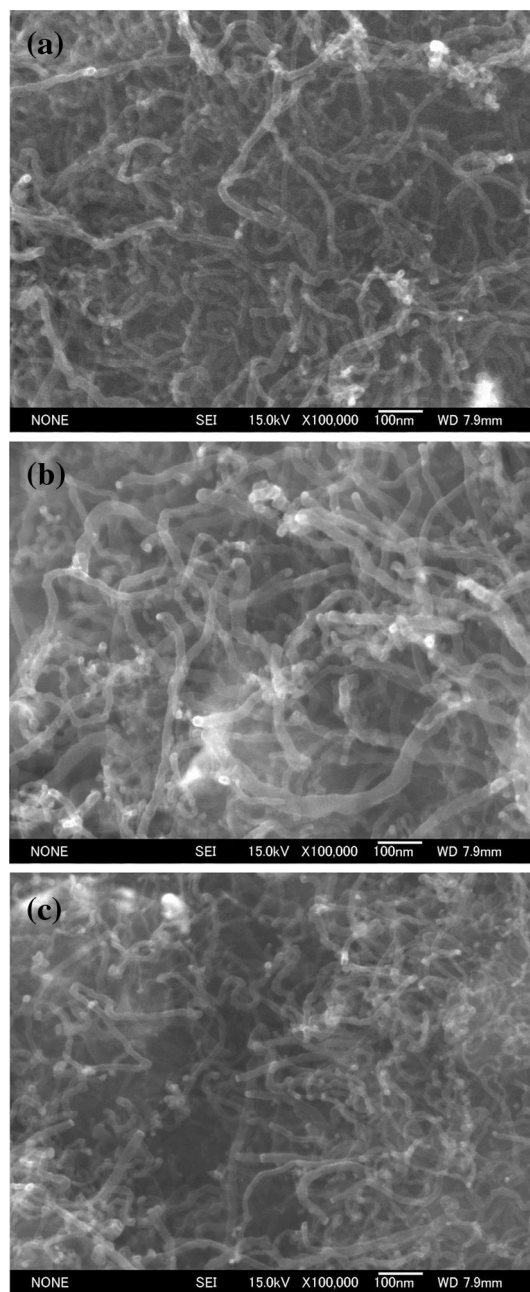

Fig. 2 SEM images of N-CNFs synthesized at 400 °C with a N–O, b N–R, and c N–I catalysts

from $Ni(NO_3)_2$, i.e., the N–O, N–R, and N–I catalysts, were used, larger growth rates were obtained in all of the calcination atmospheres. In particular, the N–R catalyst provided the largest growth rate of 61 g-CNF/g-Ni/h. Lim et al. synthesized N-CNFs with a growth rate of 6.8 g-CNF/g-catalyst/h at 400 °C, using a MgO-supported Ni–Fe catalyst with a molar ratio of Ni:Fe:MgO = 4:1:5 (Lim et al. 2009). This catalyst can contain at least 40.5 mass% Ni and 9.6 mass% Fe as the catalytic components, assuming that Ni and Fe species in the catalyst are NiO and
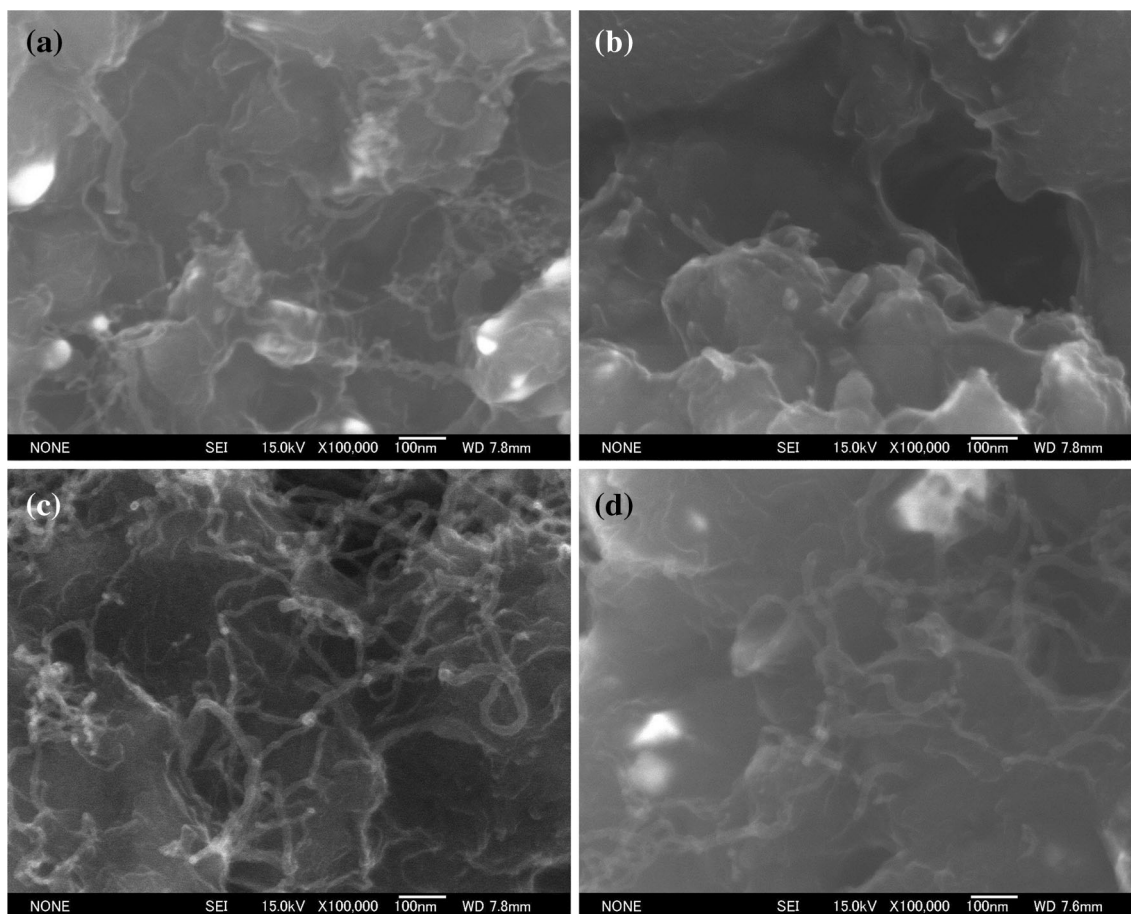
Fig. 3 SEM images of N-CNFs synthesized at 400 °C with **a** C–R, **b** S–R, **c** A–R, and **d** L–R catalysts

Fe$_2$O$_3$, respectively. Accordingly, this growth rate per unit mass of catalyst could be converted to at most 14 g-CNF/g-NiFe/h, indicating that our result using the N–R catalyst was approximately 4 times larger than this value. Figure 2 depicts the SEM images of products obtained at 400 °C using the N–O, N–R, and N–I catalysts. Regardless of the calcination atmosphere, the N-CNFs with a fiber diameter of several tens of nanometers were obtained, indicating that their morphologies were similar to those of N-CNFs synthesized by a conventional process (Kim et al. 2011). As shown in Fig. 3, however, the morphology and uniformity of N-CNFs was greatly affected by the catalyst precursors. The C-R, A-R, and L-R catalysts provided small amounts of relatively thin N-CNFs with uniform morphologies, which was probably due to low catalytic activity of the catalysts compared with the N–R catalyst. When the S-R catalyst was used, few short, thick fibers were observed, because the S-R catalyst might be deactivated by sulfur species formed via pyrolysis of nickel sulfate (Kim et al. 2006; Park et al. 2010).

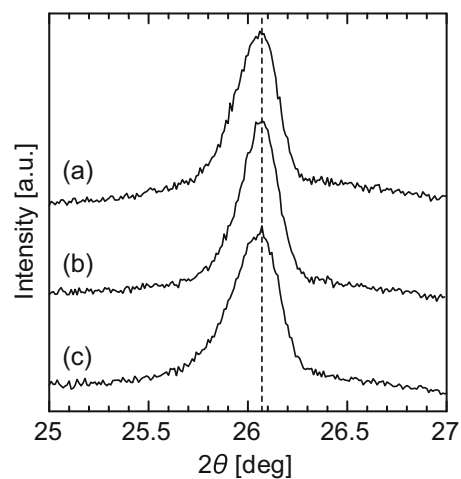Figures 4 and 5 show the XRD patterns and TG–DTA curves of products obtained at 400 °C using the N–O, N–R,

Fig. 4 XRD patterns of products synthesized at 400 °C with **a** N–O, **b** N–R, and **c** N–I catalysts

and N–I catalysts, respectively. All of the products had a diffraction peak at almost the same angle ($2\theta = 26.07°$), indicating that N-CNFs with a similar structure can be obtained using these catalysts. Furthermore, each product
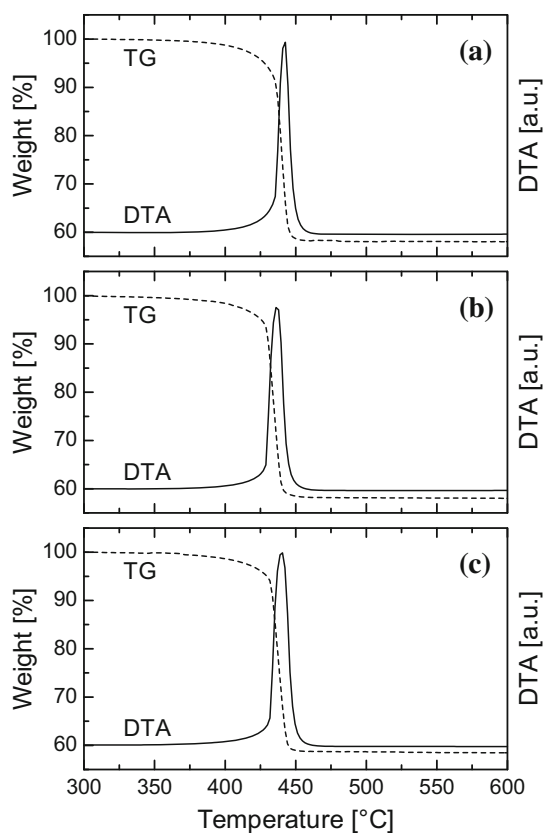
Fig. 5 TG-DTA curves of products synthesized at 400 °C with **a** N–O, **b** N–R, and **c** N–I catalysts

had a single DTA exothermic peak at approximately 440 °C, suggesting that the contents of amorphous carbon deposits in the products were very low. The nitrogen content of products obtained at 400 °C using the N–O, N–R, and N–I catalysts were 3.6, 3.8, and 3.2 at.%, respectively, which were typical values in CCVD using acetonitrile (Kim et al. 2011). Therefore, we confirmed that our catalysts can effectively yield a relatively large amount of N-CNFs even though they contain a small amount of Ni species as the catalytic component.

Variation of Ni species in catalysts with precursor and calcination atmosphere

The components of Ni species (i.e., metallic Ni and NiO) in the catalysts are expected to change depending on the precursor and the calcination atmosphere, which can vary the growth rate of N-CNFs. To confirm the phase formation of Ni species, the XRD data around the diffraction angles corresponding to the Ni(111) and NiO(220) planes, at which α-Al$_2$O$_3$ has no diffraction peaks, were collected. Figure 6 shows the XRD patterns of catalysts together with that of the Al$_2$O$_3$ support. It was confirmed that the catalysts consisted mainly of either metallic Ni or NiO as the

Ni species. The formed Ni species were found to depend strongly on the calcination atmosphere rather than the precursor. When the precursors were calcined in the oxidative and inert atmospheres, the catalysts consisting of NiO phase were obtained. Conversely, the calcination of precursors in the reductive atmosphere resulted in the formation of catalysts with metallic Ni phase. The fact that the N–O, N–R, and N–I catalysts showed the large growth rates reveals that the growth rate is independent of the Ni species in the catalysts and that the catalysts derived from Ni(NO$_3$)$_2$ possess high catalytic activity. As seen in Fig. 6, the diffraction peaks from the Ni(111) and NiO(220) planes in the N–O, N–R, and N–I catalysts broadened compared with other catalysts, implying that the crystallite sizes of Ni species in these catalysts were relatively small. Table 1 lists the average crystallite sizes of metallic Ni and NiO in all of the catalysts. The N–O, N–R, and N–I catalysts had small crystallite sizes (11.1, 12.9, and 8.8 nm, respectively) whereas the others had larger crystallite sizes between 19.6 nm and 29.7 nm. According to literature (Ren et al. 2014), Ni(NO$_3$)$_2$ can generate oxygen radicals in the thermal decomposition, which may result in the reduction of crystallite size. Figure 7 shows the relationship between the growth rate of N-CNFs at 400 °C and the crystallite size of metallic Ni or NiO. The growth rate was found to show a rough tendency to increase with decreasing crystallite size. For catalysts in which Ni species are supported on oxides, the decrease in the crystallite size of Ni species can contribute to improvement of its dispersion degree on the support, resulting in enhancement of the catalytic activity due to an increase in interaction between the Ni species and the support (Wu et al. 2013). Our catalysts may also activate according to a similar mechanism. A better understanding of the activation mechanism requires more precise investigations, which will be addressed in our future publications.

Effect of hydrogen in CVD carrier gas on N-CNF growth

Figure 8 shows the XRD patterns of N–O, N–R, and N–I catalysts after CVD in the absence of acetonitrile vapor at 400 °C. In the N–O and N–I catalysts, the diffraction peaks from the Ni(111) and NiO(222) planes were confirmed to increase and decrease, respectively, compared with the catalysts before CVD as shown in Fig. 6. Conversely, the N–R catalysts had a larger diffraction peak from the Ni(111) plane. Furthermore, when pure Ar was used as the carrier gas in the CVD process using the N–O, N–R, and N–I catalysts, the growth rates of N-CNFs were confirmed to be very small; they were less than 1 g-CNF/g-Ni/h even when the N–R catalyst was used. Accordingly, these results reveal that H$_2$ in the carrier gas plays two main roles
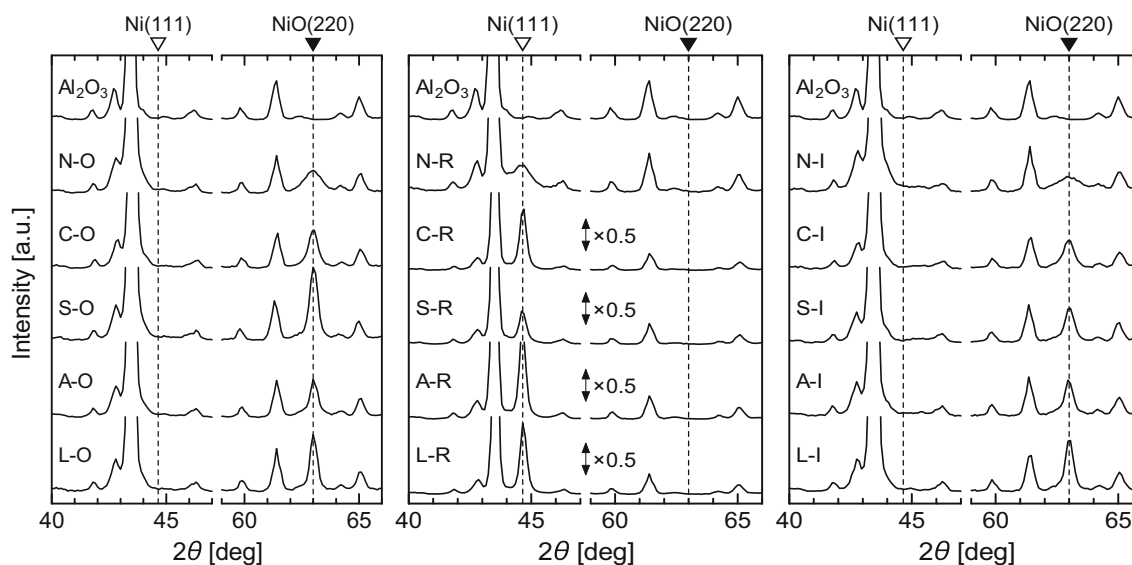
Fig. 6 XRD patterns of catalysts activated in oxidative, reductive, and inert atmospheres

Table 1 Average crystallite sizes of Ni and NiO in catalysts

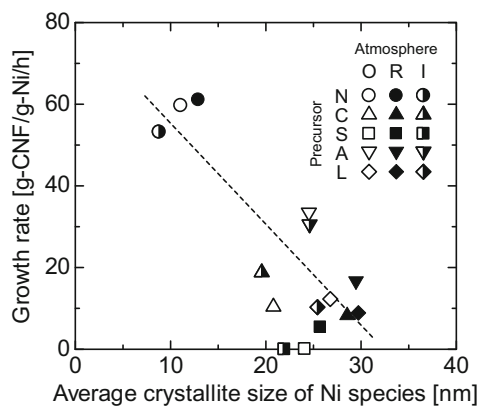| Precursor	Average crystallite size (nm)		
	Activation atmosphere		
	O: NiO(220)	R: Ni(111)	I: NiO(220)
N	11.1	12.9	8.8
C	20.8	28.5	19.6
S	24.1	25.7	21.9
A	24.5	29.5	24.6
L	24.8	29.7	25.4

Fig. 7 Relationship between growth rate of N-CNFs at 400 °C and average crystallite size of Ni species in catalysts

in the CVD process. First, H_2 can activate the catalysts by reducing NiO to metallic Ni in the catalysts, resulting in large N-CNF growth rates even when the N–O and N–I catalysts are used. Second, as Kim et al. (2011) noted, H_2
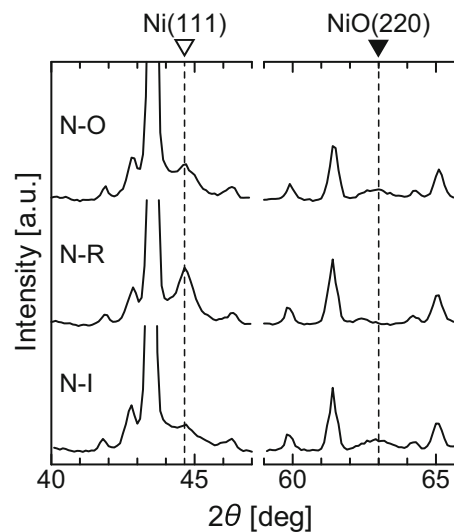

Fig. 8 XRD patterns of N–O, N–R, and N–I catalysts after CVD process in acetonitrile-free carrier gas flow at 400 °C

can prevent the catalysts from deactivating by decreasing the accumulation of excessive carbon species on the catalysts. Therefore, we can conclude that the presence of H_2 in the carrier gas effectively contributes to low-temperature synthesis of N-CNFs in an acetonitrile CCVD process using Ni-based catalysts.

CVD temperature dependence of growth rate and properties of N-CNFs

Figure 9 shows the variation in the growth rate and nitrogen content of N-CNFs with the temperature in CVD using the N–R catalyst. As the temperature was increased, the
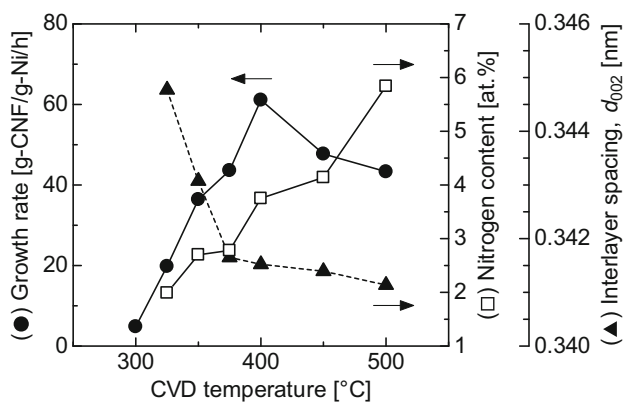
Fig. 9 Effect of reaction temperature on growth rate, nitrogen content, and interlayer spacing of N-CNFs synthesized with N–R catalyst

growth rate reached a maximum value of 61 g-CNF/g-Ni/h at 400 °C and then decreased. In contrast, the nitrogen content increased monotonically with increasing temperature. The temperature dependence of growth rate and nitrogen content is typical, and the possible mechanism can be explained based on the different diffusion rates over the catalysts of carbon species and nitrogen species, which were formed via the thermal decomposition of acetonitrile (Kim et al. 2011). Due to a lower diffusion rate of nitrogen species compared with that of carbon species at low temperatures, the deposition of carbon species on the catalysts was larger than that of nitrogen species. At high temperatures, however, the diffusion rate of nitrogen species may greatly increase compared with carbon species, resulting in an increase in the nitrogen content and a relative decrease in the growth rate.

The interlayer spacing d_{002} drastically decreased when the temperature was increased from 325 to 375 °C. At temperatures higher than 375 °C, d_{002} gradually decreased from 0.3417 nm to 0.3411 nm, which were relatively small values compared with those in a conventional method (Kim et al. 2016). This result represents that the degree of graphitization of N-CNFs can be improved above 375 °C, which may contribute to enhancement of its functionalities.

Conclusion

N-doped CNFs were synthesized at high growth rates and low temperatures in an acetonitrile catalytic CVD process using Al_2O_3-supported Ni-based (Ni/NiO) catalysts. We found that both the use of $Ni(NO_3)_2$ as the catalyst precursor and H_2-containing Ar as the carrier gas of acetonitrile vapor in CVD could contribute effectively to enhancement of the catalytic activity, resulting in high growth rates of 57 ± 4 g-CNF/g-Ni/h at 400 °C—

approximately 4 times larger than the growth rate in a conventional process. The morphology and nitrogen content of our N-CNFs were almost the same as those of N-CNFs prepared by a conventional process. The growth rate and nitrogen content depended on the temperature in CVD due to the different diffusion rates of carbon species and nitrogen species formed by the thermal decomposition of acetonitrile over the catalysts. The Ni-based catalysts can be prepared relatively easily from inexpensive materials and may be used for operating CVD reactors at low temperatures, leading to cost reductions in the production of N-CNFs.

References

Ashfaq M, Verma N, Khan S (2016) Copper/zinc bimetal nanoparticles-dispersed carbon nanofibers: a novel potential antibiotic material. Mater Sci Eng C 59:938–947. doi:10.1016/j.msec.2015.10.079

Buan MEM, Muthuswamy N, Walmsley JC, Chen D, Rønning M (2016) Nitrogen-doped carbon nanofibers on expanded graphite as oxygen reduction electrocatalysts. Carbon 101:191–202. doi:10.1016/j.carbon.2016.01.081

Cheng X, Zhang Q, Wang H, Tian G, Huang J, Peng H, Zhao M, Wei F (2015) Nitrogen-doped herringbone carbon nanofibers with large lattice spacings and abundant edges: catalytic growth and their applications in lithium ion batteries and oxygen reduction reactions. Catal Today 249:244–251. doi:10.1016/j.cattod.2014.10.047

Desmaris V, Saleem MA, Shafiee S (2015) Examining carbon nanofibers: properties, growth, and applications. IEEE Nanotechnol Mag 9:33–38. doi:10.1109/MNANO.2015.2409394

Erdem A, Eksin E, Congur G (2015) Indicator-free electrochemical biosensor for microRNA detection based on carbon nanofibers modified screen printed electrodes. J Electroanal Chem 755:167–173. doi:10.1016/j.jelechem.2015.07.031

Feng L, Xie N, Zhong J (2014) Carbon nanofibers and their composites: a review of synthesizing, properties and applications. Materials 7:3919–3945. doi:10.3390/ma7053919

Gao X, Lan J, Jia X, Cai Q, Yang X (2016) Improving interfacial adhesion with epoxy matrix using hybridized carbon nanofibers containing calcium phosphate nanoparticles for bone repairing. Mater Sci Eng C 61:174–179. doi:10.1016/j.msec.2015.12.033

Iwasaki T, Tomisawa M, Nakamura H, Watano S (2013) Synthesis of nitrogen-doped carbon nanocoils via one-step acetonitrile catalytic CVD using a Ni–Fe layered double hydroxide as catalyst precursor. Chem Vap Depos 19:323–326. doi:10.1002/cvde.201204018

Iwasaki T, Tomisawa M, Yoshimura T, Nakamura H, Ohyama M, Asao K, Watano S (2015) Synthesis of nitrogen-doped carbon

nanocoils with adjustable morphology using Ni–Fe layered double hydroxides as catalyst precursors. Nanomater Nanotechnol 5:3. doi:10.5772/60021

Jiang X (2014) CVD growth of carbon nanofibers. Phys Status Solidi A 211:2679–2687. doi:10.1002/pssa.201431631

Kim P, Kim H, Joo JB, Kim W, Song IK, Yi J (2006) Effect of nickel precursor on the catalytic performance of Ni/Al$_2$O$_3$ catalysts in the hydrodechlorination of 1,1,2-trichloroethane. J Mol Catal A Chem 256:178–183. doi:10.1016/j.molcata.2006.04.061

Kim J, Lim S, Kim S, Peck D, Lee B, Yoon S, Jung D (2011) Electrochemical catalytic activity for oxygen reduction reaction of nitrogen-doped carbon nanofibers. J Nanosci Nanotechnol 11:6350–6358. doi:10.1166/jnn.2011.4443

Kim J, Jang J, Peck D, Lee B, Yoon S, Jung D (2016) Control of nitrogen content and its effects on the electrochemical behavior of nitrogen-doped carbon nanofibers. J Electroanal Chem 768:34–40. doi:10.1016/j.jelechem.2016.02.032

Lim S, Yoon S, Mochida I, Jung D (2009) Direct synthesis and structural analysis of nitrogen-doped carbon nanofibers. Langmuir 25:8268–8273. doi:10.1021/la900472d

Liu J, Harris AT (2010) Synthesis of multiwalled carbon nanotubes on Al$_2$O$_3$ supported Ni catalysts in a fluidized-bed. AIChE J 56:102–113. doi:10.1002/aic.11974

Park HJ, Park SH, Sohn JM, Park J, Jeon J, Kim S, Park Y (2010) Steam reforming of biomass gasification tar using benzene as a model compound over various Ni supported metal oxide catalysts. Bioresour Technol 101:S101–S103. doi:10.1016/j.biortech.2009.03.036

Peng S, Li L, Lee JKY, Tian L, Srinivasan M, Adams S, Ramakrishna S (2016) Electrospun carbon nanofibers and their hybrid composites as advanced materials for energy conversion and storage. Nano Energy 22:361–395. doi:10.1016/j.nanoen.2016.02.001

Ren S, Shen Z, Zhang P, Wang Z, Lei Z, Pan C, Kang S, Shui H (2014) Highly dispersed Ni/SBA-15 catalysts prepared with different nickel salts as nickel precursors: effects of activation atmospheres. J Fuel Chem Technol 42:591–596. doi:10.1016/S1872-5813(14)60029-3

Song H, Shen W (2014) Carbon nanofibers: synthesis and applications. J Nanosci Nanotechnol 14:1799–1810. doi:10.1081/CR-100101954

Stout DA (2015) Recent advancements in carbon nanofiber and carbon nanotube applications in drug delivery and tissue engineering. Curr Pharm Des 21:2037–2044. doi:10.2174/1381612821666150302153406

Wu G, Zhang C, Li S, Han Z, Wang T, Ma X, Gong J (2013) Hydrogen production via glycerol steam reforming over Ni/Al$_2$O$_3$: influence of nickel precursors. ACS Sustain Chem Eng 1:1052–1062. doi:10.1021/sc400123f

Zhang L, Aboagye A, Kelkar A, Lai C, Fong H (2014) A review: carbon nanofibers from electrospun polyacrylonitrile and their applications. J Mater Sci 49:463–480. doi:10.1007/s10853-013-7705-y

Zhang B, Kang F, Tarascon J, Kim J (2016) Recent advances in electrospun carbon nanofibers and their application in electrochemical energy storage. Prog Mater Sci 76:319–380. doi:10.1016/j.pmatsci.2015.08.002